PAPER REFERENCE: 3C.101

# STUDY ON CONSTITUTIVE MODEL OF CYCLIC HARDENING PROCESS

N. Osawa [1], **Y.** Tomita [1] and K. Hashimoto [1]

[1] Department of Naval Architecture and Ocean Engineering, Osaka University,
2-1 Yamadaoka, Suita, Osaka 565-0871, JAPAN

## ABSTRACT

The micromechanical hardening rules developed by Cuitino and Ortiz *[Modelling Simul. Muter. Sci. Eng. 1 (1992) 225-2631* and Repetto and Ortiz [*Acta muter.* ***45,*** *6 (1997) 2577-2595*] are modified, and they are employed in the analysis of cyclic hardening behaviour of a Cu single crystal. A crystalline FEM theory which incorporates this hardening rule is presented. The validity of the presented theories are examined by comparing hysteresis loop shape parameters proposed by Abel *[Muter. Sci. Engng. 37 (1979) 187-2001* of the simulation result and ones of the experimental result. As results, the followings are found: i) It can be said that the constitutive relation employed in our simulation can be used in cyclic hardening behaviour analysis under the chosen condition because they give a good account of the changing nature of hysteresis loops qualitatively. ii) In our simulation, the cyclic state at which the shear deformation in the secondary systems increases rapidly coincides with the one at which Bauschinger energy parameter $\beta_E$ reaches its maximum. This leads to the assumption that PSB formation begins when the finite shear deformation occurs in the secondary systems.

## INTRODUCTION

Experimental data have conclusively demonstrated that fatigue crack nucleation is mediated by surface roughness which arises at the intersection between the surface and PSBs. The formation of PSB is an essential mechanism for fatigue fracture and the fatigue limit can be linked with the lower limit stress or strain for the formation of PSB. Strain localization and a change of dislocation structure occur after cyclic hardening is saturated. These two phenomena influence each other, and they are the prerequisite for PSB formation.

Success in developing a quantitative understanding of crack initiation process has been somewhat limited. Repetto and Ortiz *[1]* developed a micromechanical finite element model which can simulate the surface roughening mentioned above. In their approach, they entirely neglected the initial transient and presumed the PSB to be saturated from the outset. The authors [2][3] showed strain localization in the course of loading cycles can be simulated by using crystalline FEM theory. Because the hardening law used in these studies was formulated phenomenologically, it was impossible to simulate the interaction between the change in dislocation structure and strain localization. It is needed to develop a constitutive model of cyclic hardening stage which emanates directly from a clear micromechanical picture in order to understand the micromechanical aspects of PSB formation process.

In this paper, the micromechanical models developed by Cuitino and Ortiz *[4]* and Repetto and Ortiz *[1]* are modified so that we can employ them in the analysis of cyclic hardening behaviour. A crystalline FEM theory which incorporates this model is presented. We examine the propriety of the presented model and FEM theory by simulating cyclic hardening behaviour of Cu single crystal.

## CONSTITUTIVE RELATION

### *Strain Hardening during Monotonic Loading*

Throughout this paper, the label $(a),(b)$ identifies the specific slip system under consideration, and $\nu(t)$ denotes

the value of **v** at time ***t***. We assume that the main resistance to dislocation motion is posed by secondary dislocations piercing the slip plane, or forest dislocation during cyclic hardening process. Forest dislocations can be idealized as point obstacles. Pairs of such point obstacles arrest dislocations, which require a threshold resolved shear stress $s$ to overcome the barrier. The value of **s** changes by the change of the length of the link. Since the distribution of point obstacles within the glide plane is random, $s$ is a random variable. The probability density function $\tilde{f}(s,t)$ and the distribution function $\tilde{P}(s,t)$ are given by Cuitiiio and Ortiz **[4]**as

$$\tilde{f}(s,t)=2\pi n^{(a)}(t)\frac{(\alpha\mu b)^2}{s^3}\exp\left\{-\pi n^{(a)}(t)\frac{(\alpha\mu b)^2}{s^2}\right\},\ \tilde{P}(s,t)=\exp\left\{-\pi n^{(a)}(t)\frac{(\alpha\mu b)^2}{s^2}\right\}, \qquad (1)$$

where $n^{(a)}(t)$ is the area density of forest dislocation intersections with the glide plane of system $(a)$, $a$ a coefficient of order of $0.3$, $\mu$ the shear modulus, $b$ the length of the Burgers vector.

Let $f(s,t)$ denotes the probability density of **s** after the resolved shear stress has been increased monotonically to $\tau^{(a)}(t)$. Ortiz and Popov **[5]**derived a kinetic equation governing the evolution of $f(s,t)$. Cuitiiio and Ortiz **[4]**obtained analytical solutions of this equation. The solution is

$$f(s,t)=\frac{\tilde{f}(s,t)H\left[s-\tau^{(a)}(t)\right]}{1-\tilde{P}(\tau^{(a)}(t),t)}, \qquad (2)$$

where $H[x]$ is the Heaviside step function. This solution determine the analytical form of the self-hardening curve. Cuitiiio and Ortiz **[4]**derived the self-hardening modulus in system $(a)$,$h^{(aa)}(t)$ as

$$h^{(aa)}(t)=\frac{\dot{\tau}^{(a)}(t)}{\dot{\gamma}^{(a)}(t)}=h_c(t)\left(\frac{\tau^{(a)}(t)}{\tau_c^{(a)}(t)}\right)^3\left[\mathrm{Cosh}\left\{\left(\frac{\tau_c^{(a)}(t)}{\tau^{(a)}(t)}\right)^2-1\right\}\right], \qquad (3)$$

where, $\rho^{(a)}$ is the dislocation density, and $h_c^{(a)}(t)$ and $\tau_c^{(a)}(t)$ are given as

$$h_c^{(a)}(t)=\frac{\tau_c^{(a)}(t)}{\gamma_c^{(a)}(t)};\ \gamma_c^{(a)}(t)=b\rho^{(a)}(t)\frac{1}{2\sqrt{n^{(a)}(t)}},\ \tau_c^{(a)}(t)=\alpha\mu b\sqrt{\pi n^{(a)}(t)} \qquad (4)$$

$n^{(a)}$ is a function of the dislocation densities in all remaining systems. In the same manner as Cuitiiio and Ortiz **[4],** we assume that the form of $n^{(a)}$ is given as

$$n^{(a)}=\sum_{(b)}a^{(ab)}\rho^{(b)} \qquad (5)$$

$a^{(ab)}$ is $a_1$ when $a=b$, $a_2$ when the dislocations in two systems form no junctions or Hirth locks or co-planar junctions, $a_2$ when they form glissile junctions, and $a_3$ when they form sessile Lomer-Cottrell locks. The values of $a_1,a_2,a_3$ are dependent on the stacking fault energy and they are determined experimentally.

Assuming that the change in dislocation density is mainly caused by the breeding by cross-glide and pair annihilation, the equations of evolution for the dislocation densities are given by Cuitiiio and Ortiz **[4]as**

$$\rho^{(a)}(t)=\rho_{sat}\left\{1-\left(\frac{\rho_0^{(a)}}{\rho_{sat}}\exp\left(-\frac{\gamma^{(a)}(t)}{\gamma_{sat}}\right)\right)\right\} \qquad (6)$$

where $\rho_{sat}$ is the saturation density at which the rate of annihilation balances the rate of production, $\gamma_{sat}$ the saturation shear strain, $\rho_0^{(a)}$ the initial dislocation density in system $(a)$,and $\gamma^{(a)}$ the shear strain in system $(a)$.

When we define the flow stress $g'''$ as the elastic limit, the increase of $g'''$ due to the shear deformation in remaining systems can be neglected (Cuitiiio and Ortiz **[4]**). The flow rule is given as

$$\dot{g}^{(a)}=h^{(aa)}\dot{\gamma}^{(a)} \qquad (7)$$

***Strain Hardening during Reloading***

The Bauschinger effect was modeled within the context of the forest theory of hardening by Ortiz and Popov **[5]**. They argued that reversed slip gradually causes the dislocation / obstacle arrangement to dissolve, with the result that $f(s,t)$ approaches the virgin distribution $\tilde{f}(s)$ when the reverse slip strain $\gamma_{rev}^{(a)}$ in system $(a)$ exceeds $\gamma_c^{(a)}$. This causes the Bauschinger effect.

Assuming that $f(s,t)$ during reloading remains of the form of Eq. (2), Repetto and Ortiz [1] derived the evolution law of the critical resolved shear stress in system *(a)* for reloading, $g_0^{(a)}$. The result is

$$\widetilde{P}\left(g_0^{(a)}\right)=\frac{\widetilde{P}\left(\tau_{\max}^{(a)}\right)\exp\left(-\gamma_{rev}^{(a)}/\gamma_c^{(a)}\right)}{1+\widetilde{P}\left(\tau_{\max}^{(a)}\right)\left\{\exp\left(-\gamma_{rev}^{(a)}/\gamma_c^{(a)}\right)-1\right\}} \tag{8}$$

where, $\tau_{\max}^{(a)}$ is the maximum resolved shear stress in system *(a)* during preloading. When $\gamma_{rev}^{(a)}=0$ this equation gives $g_0^{(a)}=\tau_{\max}^{(a)}$, whereas for $\gamma_{rev}^{(a)}/\gamma_c^{(a)}>>1$ it gives $g_0^{(a)}\to 0$.

It is a well-known experimental result that $\rho^{(a)}$ increases in the course of loading history and eventually a saturation stage is reached wherein $\rho^{(a)}$ attains a constant. During the transient stage, the ratio of yield point to stress amplitude decreases gradually. Let $\gamma_{acc}^{(a)}$ denotes the accumulated shear strain in system *(a)*, $\int_{s=0}^{t}\left|\dot{\gamma}^{(a)}(s)\right|ds$. In our simulation, we use $\gamma_{acc}^{(a)}$ instead of $\gamma^{(a)}$ or $\gamma_{rev}^{(a)}$ in Eqs. **(6)** and (8). By these modifications, the changing natures of $\rho^{(a)}$ and stress-strain relation mentioned above can be expressed.

***Constitutive Equations***

The constitutive equation used in our analysis is based on the rate-dependent crystalline plasticity theory developed by Peirce, Asaro and Needleman **[6]**. It gives the relation between the Jaumann rate of Kirchhoff stress rate $\overset{\nabla}{\boldsymbol{\tau}}$, the shear rate in system *(a)* $\dot{\gamma}^{(a)}$ and the total rate of stretching, **D** as

$$\overset{\nabla}{\boldsymbol{\tau}}=\mathrm{L}:\mathrm{D}-\sum_{(a)}\dot{\gamma}^{(a)}\mathrm{R}^{(a)}\;;\quad \mathrm{R}^{(a)}=\mathrm{L}:\mathrm{P}^{(a)}+\boldsymbol{\beta}^{(a)}, \tag{9}$$

where

$$\mathbf{P}^{(a)}=\frac{1}{2}\left(\mathbf{s}^{*(a)}\otimes\mathbf{m}^{*(a)}+\mathbf{m}^{*(a)}\otimes\mathbf{s}^{*(a)}\right),\ \mathbf{W}^{(a)}=\frac{1}{2}\left(\mathbf{s}^{*(a)}\otimes\mathbf{m}^{*(a)}-\mathbf{m}^{*(a)}\otimes\mathbf{s}^{*(a)}\right) \tag{10}$$

$$;\ \mathbf{s}^{*(a)}=\mathbf{F}^{*}\mathbf{s}^{(a)},\quad \mathbf{m}^{*(a)}=\mathbf{F}^{*-T}\mathbf{m}^{(a)},\quad \boldsymbol{\beta}^{(a)}=\mathbf{W}^{(a)}\boldsymbol{\tau}-\boldsymbol{\tau}\mathbf{W}^{(a)}$$

**F*** is the elastic deformation gradient which represents elastic stretching and rigid rotation; $\mathbf{s}^{(a)}$ and $\mathbf{m}^{(a)}$ are the unit vectors in the direction of slip and the unit normal vector of the slip plane of slip system *(a)* in the undeformed configuration; **L** is the elastic moduli tensor.

We adopt the convention of differentiating between the positive and negative slip directions for each slip system, whereupon the shear rates can be constrained to be nonnegative. We define the flow stress g"" as the elastic limit. In this case, we can use the form of $\dot{\gamma}^{(a)}$ proposed by Cuitiiio and Ortiz **[4]**

$$\dot{\gamma}^{(a)}(t)=\dot{\gamma}_0\left\{\left(\frac{\tau^{(a)}(t)}{g^{(a)}(t)}\right)^{1/m}-1\right\}H\left[\tau^{(a)}(t)-g^{(a)}(t)\right], \tag{11}$$

where, $m$ is the material rate sensitivity exponent and $\dot{\gamma}_0$ is the reference shear rate. The evolution law of $g^{(a)}$ is given in Eqs. (7) and (8).

**NUMERICAL METHOD**

***Finite Element Method***

Boundary value problems in this theory can be solved using the finite element method. In the same manner as Pierce, Asaro and Needleman **[6],** analysis is based on the Lagrangian formulation with the initial unstressed state taken as reference. Also adopted is the convected coordinate formulation (Needleman [7]). Hereafter, the contravariant and covariant components of tensors or vectors on the deformed convected coordinates is abbreviated to 'cont. comp.' and 'cov. comp.'. Similarly, the components on the reference Cartesian coordinates is abbreviated to 'ref. comp.'.

***Time Integration Algorithm***

In order to calculate the cyclic deformation behaviour during fatigue process over great many loading steps, an iterative time integration algorithm by which the residual force is dispelled at every step has been developed.

From Eq. (9), the resolved shear stress and its rate can be written as

$$\tau^{(a)} = \mathbf{P}^{(a)}:\boldsymbol{\tau}\,,\ \dot{\tau}^{(a)} = \mathbf{R}^{(a)}:\Big(\mathbf{D} - \sum\nolimits_{(b)} \dot{\gamma}^{(b)}\mathbf{P}^{(b)}\Big). \tag{12}$$

The slip increment on slip system $(a)$, $\Delta\gamma^{(a)}$, with the time increment $\Delta t$ is calculated by a linear interpolation of the shear rates at time $t$ and $t+\Delta t$

$$\Delta\gamma^{(a)} / \Delta t = (1-\theta)\dot{\gamma}^{(a)}\Big|_t + \theta\dot{\gamma}^{(a)}\Big|_{t+\Delta t} \quad (0 \le \theta \le 1)\,. \tag{13}$$

$\dot{\gamma}^{(a)}|_{t+\Delta t}$ is approximated by the Taylor expansion of Eq. (11) to the first order in the incremental quantities as

$$\dot{\gamma}\big|_{t+\Delta t} = \dot{\gamma}\big|_t + \frac{\partial\dot{\gamma}^{(a)}}{\partial\tau^{(a)}}\Big|_t \Delta\tau^{(a)} + \frac{\partial\dot{\gamma}^{(a)}}{\partial g^{(a)}}\Big|_t \Delta g^{(a)}. \tag{14}$$

In Eq. (12), the cov. comp. of $\mathbf{D}$; $\overline{D}_{ij}$ can be represented by the nodal displacement rate $\dot{U}^J$ as

$$\overline{D}_{ij} = \sum\nolimits_J \overline{V}_{ij}^{\,J}\dot{U}_J\ ;\ \overline{V}_{ij}^{\,J} = \frac{1}{2}\left(F_{ki}B_{kj}^J + F_{kj}B_{ki}^J\right),\ F_{ij} = \delta_{ij} + u_{i,j},\ u_{i,J} = \sum\nolimits_J B_{ij}^J U_J\,, \tag{15}$$

where, $F_{ij}$ is the ref. comp. of the total deformation gradient, $u_i$ is the ref. comp. of the deformation vector and $B_{ij}^J$ is the gradient of the shape function. By using Eq. (15) and integrating Eq. (12)$_2$, $\Delta\tau^{(a)}$ can be given by the nodal displacement increment $\Delta U_J$ and the shear increment $\Delta\gamma^{(a)}$. By integrating Eq. (10), $\Delta g^{(a)}$ can be written by $\Delta\gamma^{(a)}$.

In the following, the summations $\Sigma_{(a)}, \Sigma_{(b)}$ are taken for all active systems. Substituting Eq. (14) and the equations for $\Delta\tau^{(a)}$ and $\Delta g^{(a)}$ into Eq. (13), the relation between the slip increments and the nodal displacement increments are derived as

$$\Delta\gamma^{(a)} = \dot{f}^{(a)} + \overline{F}^{(a)ij}\sum\nolimits_J \overline{V}_{ij}^{\,J}\big|_t\,\Delta U_J\ ;\ \dot{f}^{(a)} = \sum_{(b)} M_{ab}\dot{\gamma}^{(b)}\Big|_t\,,\ \overline{F}^{(a)ij} = \sum_{(b)} M_{ab}\overline{Q}^{(b)ij}, \tag{16}$$

where,

$$\overline{Q}^{(a)ij} = \Delta t\theta\frac{\dot{\gamma}_0}{m}\left(\frac{\tau^{(a)}}{g^{(a)}}\right)^{1/m}\frac{1}{\tau^{(a)}}\overline{R}^{(a)ij}\Big|_t\ ,\ \left[M_{ab}\right] = \left[N_{ab}\right]^{-1}. \tag{17}$$

$\overline{R}^{(a)ij}$ is the cont. comp. of $\mathbf{R}^{(a)}$ in Eq. (9). $N_{ab}$ is given as

$$N_{ab} = \delta_{ab} + \theta\Delta t\frac{\dot{\gamma}_0}{m}\left(\frac{\tau^{(a)}|_t}{g^{(a)}|_t}\right)^{1/m}\left(\frac{1}{\tau^{(a)}|_t}\mathbf{R}^{(a)}|_t:\mathbf{P}^{(b)}|_t + \frac{1}{g^{(a)}}h^{(ab)}\delta_{ab}\right). \tag{18}$$

Integrating the constitutive equation (9) with respect to time and substituting Eq. (16) into this integrated equation, a set of equations for the cont. comp. of the Kirchhoff stress, $\overline{\tau}^{ij}$ and the nodal displacement $U_J$ at $t$ and $t+\Delta t$ is derived

$$\begin{aligned}
&\varphi^{ij} = \left(\overline{\tau}^{ij}\big|_{t+\Delta t} - \overline{\tau}^{ij}\big|_t\right) - \sum_J \overline{G}_J^{ij}\left(U_J\big|_{t+\Delta t} - U_J\big|_t\right) + \sum_{(a)}\dot{f}^{(a)}\overline{R}^{(a)ij}\Big|_t\,\Delta t = 0 \\
&;\ \overline{G}_J^{ij} = \left(\overline{L}^{ijkl}\big|_t - \overline{g}^{ik}\big|_t\,\overline{\tau}^{jl}\big|_t - \overline{g}^{jl}\big|_t\,\overline{\tau}^{ik}\big|_t - \sum_{(a)}\overline{R}^{(a)ij}\Big|_t\,\overline{F}^{(a)kl}\Big|_t\right)\cdot\frac{1}{2}\left(F_{mk}\big|_t\,B_{ml}^J + F_{ml}\big|_t\,B_{mk}^J\right),\ u_{i,J} = \sum\nolimits_J B_{ij}U_J
\end{aligned} \tag{19}$$

where $\overline{L}^{ijkl}$ and $\overline{g}^{ij}$ are the cont. comp. of the elastic moduli and the metric tensor.
The principle of virtual work at $t+\Delta t$ leads to

$$\Psi_J = \int_V \overline{\tau}^{ik}\Big|_{t+\Delta t}\left(\delta_{jk} + \sum_L B_{jk}^L U_L\big|_{t+\Delta t}\right)B_{ji}^J dV - F_J\big|_{t+\Delta t} = 0\ ;\ F_J\big|_{t+\Delta t} = \int_{S_t} T^i\Big|_{t+\Delta t} N_j^J dS. \tag{20}$$

Here, $T_i$ is the ref. comp. of the nominal traction on the surface. $V$ and $S$ are the volume and the surface of the body in the reference configuration.

Taking the first approximation of $\overline{\tau}^{ij}|_{t+\Delta t}$ and $U_J|_{t+\Delta t}$ as of $\overline{\tau}^{ij}|_{t+\Delta t} = \overline{\tau}^{ij}|_t$ and $U_J|_{t+\Delta t} = U_J|_t$, two sets of successive iterations for $\overline{\tau}^{ij}|_{t+\Delta t}$ and $U_J|_{t+\Delta t}$ can be derived by using the Newton-Raphson procedure for Eqs. (19) and (20)

$$\delta U_J\big|_{t+\Delta t} = \sum_L\left(\left[S_{JL}\right]^{-1}\right)_{JL}\left(-\Psi_L + F_L^v\right),\ \delta\overline{\tau}^{ij}\Big|_{t+\Delta t} = -\varphi^{ij} + \sum_J \overline{G}_J^{ij}\,\delta U_J\big|_{t+\Delta t} \tag{21}$$

where,

$$S_{JL} = \int_V\left(\overline{\tau}^{ik}\Big|_{t+\Delta t}B_{jk}^L B_{ji}^J + F_{kj}\Big|_{t+\Delta t}B_{ki}^J\overline{G}_L^{ij}\right)dV\ ,\ \ F_J^v = \int_V F_{kj}\Big|_{t+\Delta t}B_{ki}^J\varphi^{ij}dV\,. \tag{22}$$

*[S,,,,]*in Eq. (22) corresponds to the stiffness matrix.

***Determination of the Active Slip Systems***

In the previous subsection, the set of active systems has been presumed known. Let A denotes the active system set. A can be determined by the iterative algorithm proposed by Cuitiiio and Ortiz [4]. The procedure is as follows: i) A is initialized as NULL; ii) Compute **Ay'"'** based on current A; iii) Update state variables based on current $\Delta\gamma^{(a)}$; iv) If $\tau^{(a)}|_{t+\Delta t} < g^{(a)}|_{t+\Delta t}$ for $\forall(a)$ **P** *A* exit; v) If not $\tau^{(a)}|_{t+\Delta t} < g^{(a)}|_{t+\Delta t}$ for $\forall(a)$ **P** A, add most loaded system to A and repeat ii)-v).

## SIMULATION OF CYCLIC HARDENING BEHAVIOUR

***Nature of Cyclic Hardening Behaviour***

Stress half amplitude $\sigma_p$ and 'Bauschinger energy parameter', $\beta_E$ proposed by Abel [8] are good indicators of the changing nature of the hysteresis loops during cyclic hardening stage. As shown in Figure 1, $\beta_E$ is defined as

$$\beta_E = \frac{2\sigma_p \Delta\varepsilon_{pl} - \oint \sigma d\varepsilon}{\oint \sigma d\varepsilon}, \qquad (23)$$

where, $\Delta\varepsilon_{pl}$ is the nominal plastic strain amplitude, $\sigma$ the nominal stress and $\varepsilon$ the nominal (total) strain. $\beta_E$ reflects the yield lowering as well as the strain hardening characteristics. The value of $\beta_E$ approaches zero when the hysteresis loop shape approaches that of a parallelogram, whereas the more pointed the hysteresis loop shape the higher is the value of $\beta_E$.

Abel [8] performed the constant plastic strain amplitude cyclic loading tests on Cu single crystals. He found the followings: i) At the first few cycles, rectangular shaped hysteresis loops were produced with negligible values of $\beta_E$; ii) With further cycling, cyclic hardening leaded to increased $\sigma_p$ and a rapid growth in $\beta_E$; iii) When $\beta_E$ had the maximum value, slip lines were observed to appear on the specimen surface, and thus this cyclic state coincided with the beginning of PSB formation; iv) With further cycling, strain localized and PSBs were developing; v) The development of PSBs finished when $\sigma_p$ reached its maximum.

***Model Perspectives***

We apply the theory mentioned in the previous sections to the simulation of cyclic hardening behaviour of a Cu single crystal subjected to constant strain amplitude pulsating cyclic loading. When the simulation results give a good account of the changing nature of $\sigma_p$ and $\beta_E$ mentioned previous subsection, it can be supposed that it is good to employ the theory in the cyclic hardening behaviour analysis.

In this paper, we focus on the response during the period before $\beta_E$ reaches its maximum. In this case, we can approximate that deformation of a crystal is uniform, therefore, the simulation is performed using a single eight-node brick finite element. The tensile direction is aligned with the element axes. The two loaded faces of the cube are constrained to remain parallel to each other and perpendicular to the loading axis. The elasticity of the crystal is taken as isotropic. The values of the material constants employed in the simulation are listed in Table 1. Except for $\gamma_{sat}$, the properties of pure copper are used in Table 1. In order to reduce the calculation time, the value of $\gamma_{sat}$ in Table 1 is selected so that the dislocation density in all active systems becomes constant by about 200 cycles. This is about 10 times as fast as that of real material.

We shall distinguish each slip systems by the identifier listed in Table 2. The loading direction is set so that it deviates slightly from [112]. Schimid factors of each systems are shown in Table 3. C5 is the primary system and D4 is the conjugate one.

The parameter $\theta$ in Eq. (13) is *0.5*. End displacement is controlled so that the nominal strain rate is $10^{-4}[1/s]$. The nominal strain amplitude is $2.04 \times 10^{-3}$. The number of loading cycles is 230. We call the period from the beginning of the loading to the first maximum tensile loading 'the 0th cycle', and the period from the $i$ th maximum tensile loading to the $i+1$ th maximum tensile loading 'the i th cycle'.

***Simulation Result and Discussion***

Figure 2(a) shows the computed nominal stress-strain curves during the period from the 0th to the 20th cycle, and Figure 2(b) shows ones during the period from the 21st to the 230th cycle. Figure 3 and 4 show the relations of number of cycles to $\sigma_p$ and $\beta_E$. The followings are shown in these figures. i) Initially $\sigma_p$ increases rapidly and reach a maximum at the 3rd cycle, then decreases slowly and reach a minimum at the 20th cycle. ii) Rectangular shaped hysteresis loops were produced with negligible values of $\beta_E$ at the first 20 cycles. iii) From the 20th to the 120th cycle, the hysteresis loop shape becomes more pointed, and both $\sigma_p$ and $\beta_E$ increase. iv) At the 120th cycle, $\beta_E$ reaches its maximum value whereas $\sigma_p$ continues to increase. v) At the 150th cycle, $\sigma_p$ reaches its maximum value.

Let $S_{,,}$ and $\overline{\beta}_E$ denote the normalized values of $\sigma_p$ and $\beta_E$, and $\overline{N}$ denote the normalized number of cycles. $S_{,,,}$ $\overline{\beta}_E$ and $\overline{N}$ are normalized between the values corresponding to the minimum and the maximum values of $\overline{\sigma}_p$. In the experiment of Abel [8], plastic strain amplitude was held $2.2 \times 10^{-3}$. In this experiment, single-slip direction was employed and dislocation multiplication was saturated after more than $10^3$ cycles. This strain amplitude corresponds to the one of our simulation, but the loading direction and the value of $\gamma_{sat}$ are different from ones employed in our simulation. Because of these differences, we cannot make a quantitative comparison of the experimental and our simulation results. Therefore, we shall compare the relations of $\overline{N}$ to $S_{,,}$ and $\overline{\beta}_E$. Figure 5 shows the relation of $\overline{\sigma}_p$ to $\overline{N}$, and Figure 6 shows the one of $\overline{\beta}_E$ to $\overline{N}$. These figures show that the changing nature of $\sigma_p$ and $\beta_E$ gives a good account of the nature of the experimental result qualitatively except for first few cycles. From these results, it can be said that the constitutive relation employed in our simulation can be used in cyclic hardening behaviour analysis under the chosen condition.

The relation of cycle number to the accumulated shear strain $\gamma_{acc}^{(a)}$ of each systems are shown in Figure 7. This figure shows that the shear deformation on the secondary systems, A6, A3, D1 and C1, gradually increase as cyclic hardening proceeds, and this increase becomes more notable approximately at the 100th cycle. This cyclic state coincides with the one at which $\beta_E$ reaches its maximum. According to the experimental results, PSB formation begins at this stage. These results lead to the assumption that PSB formation begins when the finite shear strain occurs in the secondary systems. The formation of PSBs is a poorly understood phenomenon. In many potent theories (e.g. Kuhlmann-Wilsdorf and Laird [9]), they have assumed that PSB is formed from the dislocation structure made by the activation of secondary systems. The inference mentioned above drawn from our simulation result is consistent with these theories.


1. Repetto E.A. and Ortiz M. [1]Acta mater. **45,** 6 (1997) pp. 2577-2595.
2. Osawa N., Tomita **Y.** and Hashimoto K. Proc. 8th Int. Offshore and Polar Eng. conf. IV (1998) pp. 347-352.
3. Osawa N., Tomita **Y.** and Hashimoto K. Proc. ECF12 II (1998) pp. 969-974.
4. Cuitiiio A.M. and Ortiz M. Modelling Simul. Mater. Sci. Eng. **1**(1992) pp.225-263.
5. Ortiz M. and Popov E.P. Proc. R. Soc. Lond. **A** 379 (1982) pp.439-458.
6. Peirce D., Asaro R.J. and Needleman A. Acta Metall. **31** (1983) pp. 1087-1l 19.
7. Needleman A. Brown University Report MRL E-134 (1981).
8. Abel A. Mater. Sci. Eng. **A** 164 (1993) pp.220-225.
9. Kuhlmann-Wilsdorf D. and Laird C. Mater. Sci. Engng **46** (1980) p.209

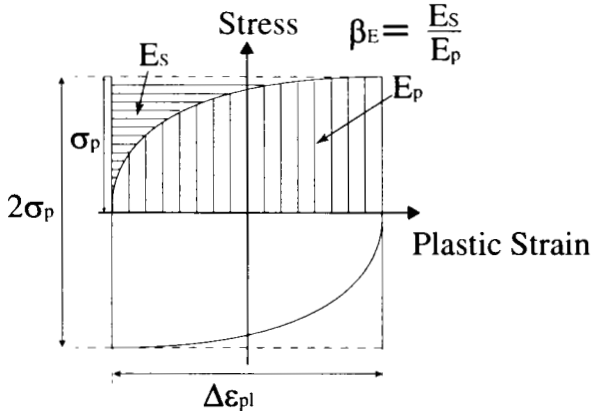


**Figure 1:** Bauschinger energy parameter

TABLE 1: Material Properties

| | |
|---|---|
| Young's modulus $E$ | 122.5E3 (MPa) |
| Poison's ratio v | 0.33 |
| $a$ of Eq. (1) | 0.3 |
| Length of Burgers vector $b$ | 2.56E-10 (m) |
| $\dot{\gamma}_0$ in Eq. (16) | 1.0 |
| $m$ in Eq. (16) | 0.01 |
| Initial value of $g$ in Eq. (16) | 2.0 (MPa) |
| $p_0$ in Eq. (9) | 1E12 |
| $p_n$ in Eq. (9) | 1E14 |
| $\gamma_{sat}$ in Eq. (9) | 0.001 |
| $a_0$ for $a^{(ab)}$ in Eq. (8) | 7.5E-4 |
| $a_1$ for $a^{(ab)}$ in Eq. (8) | $5.7\times a_0$ |
| $a_2$ for $a^{(ab)}$ in Eq. (8) | $10.2\times a_0$ |
| $a_3$ for $a^{(ab)}$ in Eq. (8) | $16.6\times a_0$ |

TABLE 2: Slip systems of f.c.c. a crystal

| | | | | | |
|---|---|---|---|---|---|
| 1 | A2 | $(111)[1\bar{1}0]$ | 7 | B2 | $(11\bar{1})[1\bar{1}0]$ |
| 2 | A6 | $(111)[01\bar{1}]$ | 8 | B5 | $(11\bar{1})[011]$ |
| 3 | A3 | $(111)[10\bar{1}]$ | 9 | B4 | $(11\bar{1})[101]$ |
| 4 | D1 | $(\bar{1}11)[110]$ | 10 | C1 | $(1\bar{1}1)[110]$ |
| 5 | D6 | $(\bar{1}11)[01\bar{1}]$ | 11 | C5 | $(1\bar{1}1)[011]$ |
| 6 | D4 | $(\bar{1}11)[101]$ | 12 | C3 | $(1\bar{1}1)[10\bar{1}]$ |

TABLE 3: Schmid factors of slip systems

| | | | | | |
|---|---|---|---|---|---|
| 1 | A2 | 0.000217 | 7 | B2 | 0.000000 |
| 2 | A6 | 0.272274 | 8 | B5 | 0.000000 |
| 3 | A3 | 0.272057 | **9** | B4 | 0.000000 |
| 4 | D1 | 0.272057 | 10 | C1 | 0.272274 |
| 5 | D6 | 0.136083 | 11 | C5 | 0.408357 |
| 6 | D4 | 0.408140 | 12 | C3 | 0.136083 |

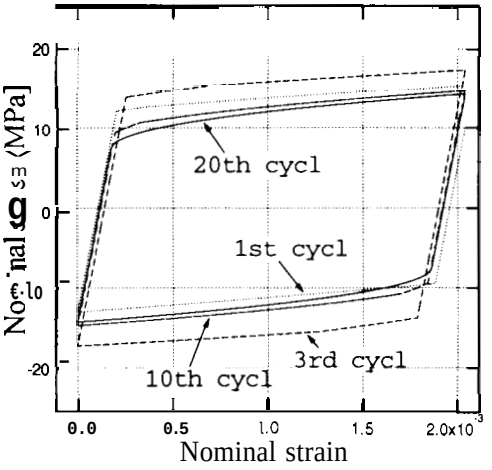


(a) The 0th -- 20th cycle

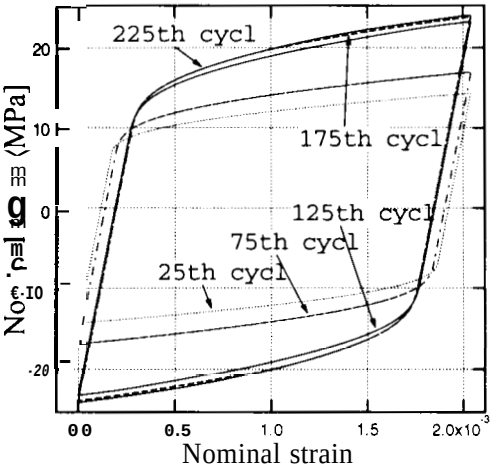


(a) The 21st -- 230th cycle

**Figure 2:** Calculated nominal stress-strain curves

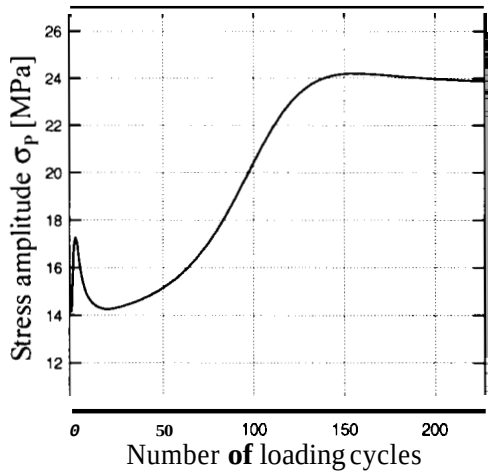


**Figure 3:** Calculated time history of stress half amplitude $\sigma_p$

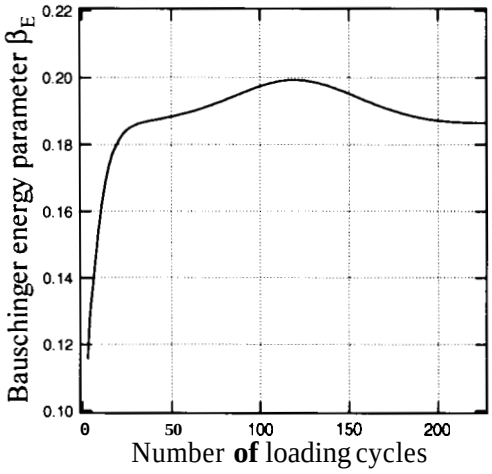


**Figure 4:** Calculated time history of Bauschinger energy parameter $\beta_E$

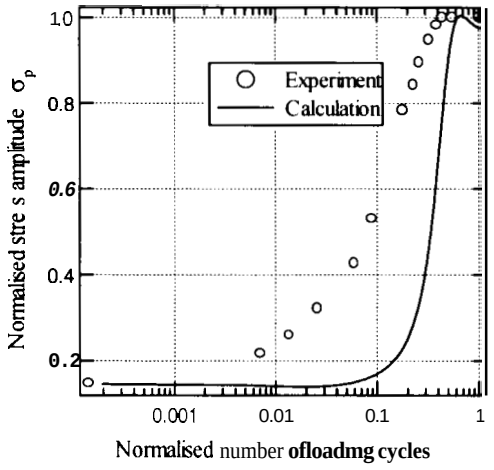


**Figure 5:** Comparison of the calculated and experimental results of stress half amplitude $\sigma_p$

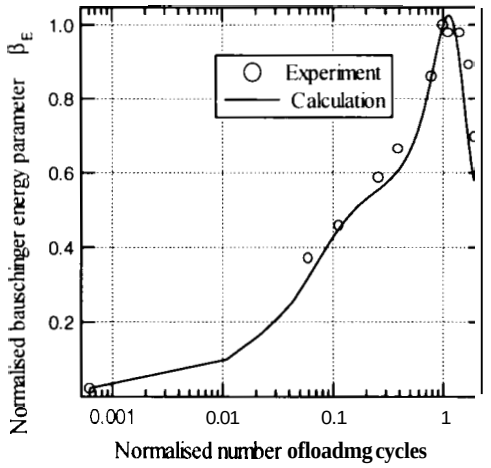


**Figure 6:** Comparison of the calculated and experimental results of Bauschinger energy parameter $\beta_E$

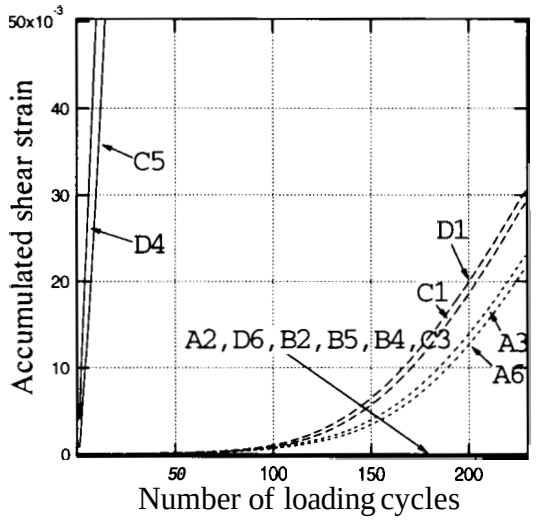


**Figure 7:** Calculated time history of the accumulated shear strain $\gamma_{acc}^{(a)}$ of each systems